

# Absence of amorphous forms when ice is compressed at low temperature

Chris A. Tulk<sup>1\*</sup>, Jamie J. Molaison<sup>1</sup>, Adam R. Makhluf<sup>2</sup>, Craig E. Manning<sup>2</sup> & Dennis D. Klug<sup>3</sup>

**Amorphous water ice comes in at least three distinct structural forms, all lacking long-range crystalline order. High-density amorphous ice (HDA) was first produced by compressing ice I to 11 kilobar at temperatures below 130 kelvin, and the process was described as thermodynamic melting<sup>1</sup>, implying that HDA is a glassy state of water. This concept, and the ability to transform HDA reversibly into low-density amorphous ice, inspired the two-liquid water model, which relates the amorphous phases to two liquid waters in the deeply supercooled regime (below 228 kelvin) to explain many of the anomalies of water<sup>2</sup> (such as density and heat capacity anomalies). However, HDA formation has also been ascribed<sup>3</sup> to a mechanical instability causing structural collapse and associated with kinetics too sluggish for recrystallization to occur. This interpretation is supported by simulations<sup>3</sup>, analogy with a structurally similar system<sup>4</sup>, and the observation of lattice-vibration softening as ice is compressed<sup>5,6</sup>. It also agrees with recent observations of ice compression at higher temperatures—in the ‘no man’s land’ regime, between 145 and 200 kelvin, where kinetics are faster—resulting in crystalline phases<sup>7,8</sup>. Here we further probe the role of kinetics and show that, if carried out slowly, compression of ice I even at 100 kelvin (a region in which HDA typically forms) gives proton-ordered, but non-interpenetrating, ice IX’, then proton-ordered and interpenetrating ice XV’, and finally ice VIII’. By contrast, fast compression yields HDA but no ice IX, and direct transformation of ice I to ice XV’ is structurally inhibited. These observations suggest that HDA formation is a consequence of a kinetically arrested transformation between low-density ice I and high-density ice XV’ and challenge theories that connect amorphous ice to supercooled liquid water.**

The phase diagram of liquid water is shown in Fig. 1a. If kept at low temperature, HDA can be recovered to ambient pressure, and upon heating transforms to a lower-density amorphous (LDA) form. Further heating results in what appears to be step-like increase in heat capacity at  $129 \pm 1$  K (this resembles a glass transition) and recrystallization into ice I at  $160 \text{ K}^{9-11}$ . Compressing LDA results in transformation back to HDA at 2 kbar. Above the glass transition, a deeply supercooled liquid water has been postulated<sup>9,12</sup>. Two deeply supercooled liquid forms corresponding to the HDA and LDA solid forms are postulated, a high-density liquid (HDL) and a low-density liquid (LDL), with a clearly demarcated transformation between the two. This transition curve has been extended into ‘no man’s land’, a region of the water phase diagram where only crystalline ice has been found (although recently it has been observed that rapid compression into no man’s land may result in short-lived forms of amorphous ice<sup>13</sup>). Ultimately, the concept of a second critical point in water was hypothesized and the search for experimental confirmation is currently a field of active research<sup>2</sup>. This hypothesis is challenged by the fact that bulk liquid water cooled slowly from a higher temperature crystallizes homogeneously, and that amorphous forms warmed from a lower temperature also crystallize<sup>2</sup>. In addition to HDA and LDA, very-high-density amorphous (VHDA) ice has also been experimentally observed upon temperature annealing

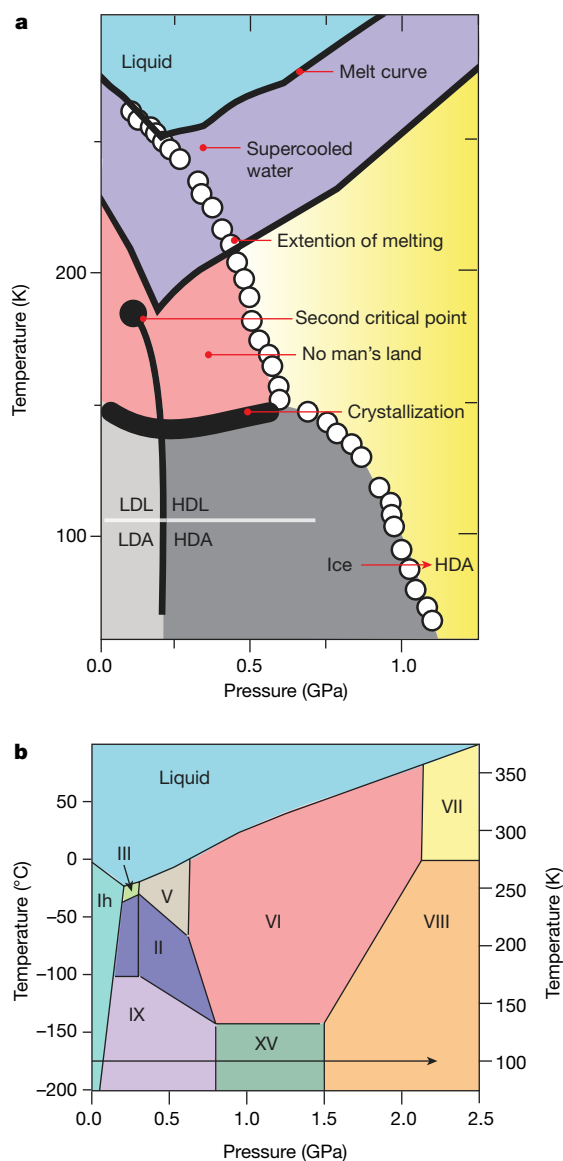
HDA under high pressure<sup>14</sup>. Analysis of X-ray radial distribution functions and Raman data measured during the transition from VHDA to LDA indicate that the local structure of LDA trends towards ice I and that of VHDA towards ice VI<sup>8,15</sup>.

Each amorphous ice form is thought to exist in its own local minimum of the overall energy landscape, with attempts made to identify the amorphous form with the lowest relative local energy minima that would represent the kinetically most stable form of amorphous ice<sup>16</sup>. Although HDA re-crystallization has also been observed<sup>17,18</sup>, the impossibility of keeping HDA isostatic and observing re-crystallization has prompted changes to the thermal conditions that effectively move the sample into other regions of the phase diagram. Our study differs from previous work in that we observe directly the lowest-energy crystal forms occurring at the conditions of HDA formation.

Above 10 kbar, the crystalline structure of ice comprises two sublattices. Each of these networks is bonded by an intra-network hydrogen-bonding arrangement with no inter-network hydrogen bonding. These forms consist of two interpenetrating networks. As such, each hydrogen-bonded network can retain a nearly ideal tetrahedral bonding arrangement while increasing the overall density to accommodate the applied pressure. These higher-temperature structures are proton-disordered and, upon cooling, should transition into energetically favoured proton-ordered structures. However, the nature of the hydrogen-bonded network means that molecular reorientations are cooperative, and as the molecular kinetics reduce upon cooling, the transformation becomes kinetically ‘frozen in’ and the ordered forms never form, with few exceptions, such as ice VIII. Doping these phases with an acid (or base) allows increased mobility upon cooling, and at least partial transformation to the ordered structure can occur. For example, doping ice V and XII with hydrochloric acid (HCl) results in ice XIII and ice XIV upon cooling. Cooling HCl-doped ice VI results in the formation of proton-ordered ice XV<sup>19,20</sup>. Both ice VI and ice XV are composed of two interpenetrating hydrogen-bonded networks. The interpenetrating nature of ice XV enables the molecules to be tetrahedrally bonded with minimal distortion of the tetrahedral angle; thus, this phase is probably the most stable ice structure in the pressure region from about 8 kbar to about 15 kbar, as indicated in the phase diagram of ice shown in Fig. 1b.

We therefore re-investigated this pressure region using a range of compression rates, with the goal of further characterizing the amorphization process and the resulting structures. A detailed outline of how each sample was prepared for this study is given in Methods. Figure 2a shows structural data collected before and after the compression of a pure sample of ice Ih at 100 K. The pressure was quickly and linearly ramped from ambient to 15 kbar at a rate of  $8.7 \text{ bar s}^{-1}$ . The data show that the initial ‘as produced’ sample is ice Ih and has no other contaminant phases. Diffraction data collected after compression show the sample to be fully amorphized HDA ice, as in previous studies. Further compression of this sample led to the transformation to a form previously denoted as ice VII’ owing to its close structural relationship

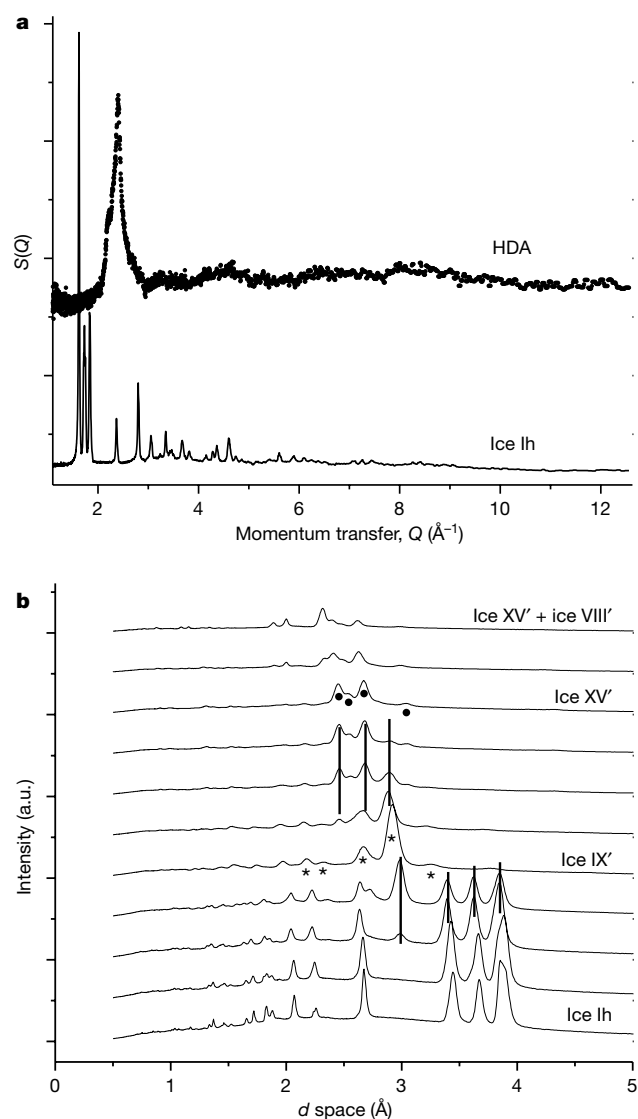
<sup>1</sup>Neutron Sciences Directorate, Oak Ridge National Laboratory, Oak Ridge, TN, USA. <sup>2</sup>Department of Earth, Planetary and Space Sciences, University of California Los Angeles, Los Angeles, CA, USA. <sup>3</sup>National Research Council of Canada, Ottawa, Ontario, Canada. \*e-mail: [tulkca@ornl.gov](mailto:tulkca@ornl.gov)



**Fig. 1 | Phase diagrams of crystalline ice and liquid and amorphous water.** **a**, Possible relationships between pressure-amorphized ice, deeply supercooled liquid water and supercooled liquid water. The transformation between crystalline ice and HDA occurs near 1.0 GPa at 100 K. In the region above about 145 K, no amorphous or liquid forms occur, and the first crystalline form is probably ice IX. The glass transitions between LDA and LDL and between HDA and HDL occur around 130 K (HDL and LDL are the deeply supercooled liquid forms). Only crystalline forms of bulk ice are observed in the pink-shaded area (no man's land), and the proposed second critical point is located within this region. **b**, Phase diagram of crystalline phases of ice in the relevant pressure ranges. The phase boundary lines indicate historical approximations of where transformations are thought to occur. The horizontal arrow represents the pressure-temperature path taken.

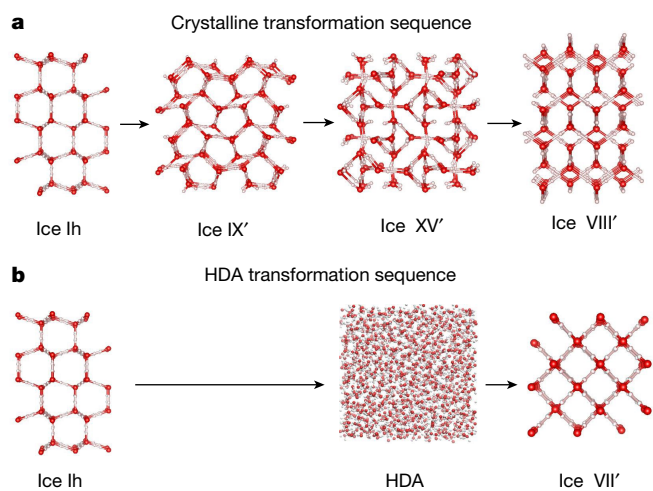
to ice VII<sup>21</sup>. We note that ice VII' is formed from two interpenetrating sublattices and is proton-disordered.

Figure 2b shows diffraction data collected during the slow compression of a pure ice Ih sample at 100 K (see Extended Data Fig. 1 for the pressure-load curve). The initial diffraction pattern shows the sample as produced, again with no sign of contaminant phases. Initial tests indicated that one of the samples may have been contaminated with ice IX seeds (which formed upon cooling), so measures were taken to ensure that the samples used to collect the data presented in Fig. 2 were phase-pure (see Extended Data Figs. 2, 3). The pressure was increased from ambient to 2.0 kbar at the same compression rate (8.7 bar s<sup>-1</sup>)



**Fig. 2 | Diffraction data of amorphous and crystalline ice for increasing pressure at 100 K.** **a**, Structure factor functions,  $S(Q)$ , of crystalline ice Ih and HDA after fast compression (see text). **b**, Diffraction data for the series of crystalline phases observed after slow compression of the sample (see text). The final result was a mixture of remnant ice XV' and ice VIII'. Vertical lines connecting datasets indicate that the hydraulic load on the sample was increased, but the sample pressure remained constant—an indication of a progressing phase transition. The main peaks of ice IX are marked by asterisks and those of ice XV by black circles. This crystalline sequence was observed in four independent datasets.

that had resulted in HDA in the previous run, but the pressure was maintained at 2 kbar and a second diffraction pattern was taken over the course of 1 h. Other than compression of the unit cell, no structural changes were observed at this point. The pressure was then increased at 8.7 bar s<sup>-1</sup> to 3.0 kbar, where the sample was again held isobarically, and another diffraction pattern was collected for 1 h. In this dataset, the initial stages of the formation of ice IX were indicated by the appearance of the most intense diffraction peak of ice IX at 2.99 Å. During the next increase in hydraulic load on a Paris-Edinburgh press, it was noted that the position of the Bragg peaks did not shift and no change in the unit cell volume was observed—an indication that the sample was progressing through a phase transition and the transformation from ice Ih to ice IX continued. The sample fully transformed to ice IX by 7 kbar. Increasing the pressure above 10 kbar resulted in the formation of ice XV', which was stable up to 30 kbar, when it transformed to ice VIII'. (We use prime notation to indicate that various studies report variable levels of proton ordering, while the overall crystal structure is similar



**Fig. 3 | Amorphous and crystalline structural progression of ice when compressed at 100 K.** **a**, Transformation of ice Ih when compressed slowly at 100 K (see text). At 3 kbar, ice Ih collapses to distorted, tetrahedrally bonded ice IX', followed by the formation of ice XV' above 10 kbar, and finally of ice VIII' above 30 kbar. **b**, Transformation sequence observed upon fast compression at 100 K (see text). Formation of ice IX is not possible on the timescale that the sample is within its stability field, and once in the field of ice XV, the kinetics is too slow to simultaneously order the protons and form an interpenetrating structure, resulting in HDA ice followed by ice VII'.

to that of pure ice XV and ice VIII, so the degree of ordering may vary.) We observed this transformation sequence in four independent experimental runs, with the additional diffraction data, along with amorphization data plotted in  $d$  space, where  $d$  is the distance between lattice planes, and data comparing ice Ih, XV' and VIII' provided in Extended Data Figs. 2, 3 and 4, respectively.

An illustration of the stepwise transformation sequence for the formation of HDA and the high-pressure crystalline phases is shown in Fig. 3. It is important to note here that on slow pressurization the progression of the crystalline phases is as follows. First, an ordering transition to ice IX' occurs and allows at least partial ordering of the water dipoles without forming an interpenetrating lattice. This is followed at higher pressure by the division of the single hydrogen-bonded network into the interpenetrating and ordered networks of ice XV'. If the stability field of ice IX' is 'stepped over' by pressurizing rapidly and directly into the field of ice XV', any resulting ordering is kinetically inhibited and the phase transformation is arrested, giving instead the highly disordered ice form known as HDA ice. Extended Data Fig. 5 shows data collected from the crystalline phases produced by rapid and slow compression.

Mapping the sequence of equilibrium structures that are seen when avoiding HDA formation provides useful insight into the structural pathway leading to pressure-induced amorphous ice. Ice IX' seems to be the key phase in this regard, in that it facilitates the transition between ice Ih and ice XV', the equilibrium crystalline structure associated with HDA. Put differently, if ice IX is not given time to form, as is the case during rapid compression, proton ordering and interpenetration of the two sublattices to form ice XV cannot occur concurrently, and HDA inevitably results. This finding challenges the interpretation of the increase in heat capacity when heating HDA to  $129 \pm 1$  K as evidence of a glass transition<sup>22</sup>. Instead, temperature annealing of amorphous ice, which is understood as a kinetically interrupted crystal-to-crystal transition, would result in the system structurally completing its unfinished transition and moving towards its more energetically favourable crystalline state at the given pressure and temperature—not to a dynamically free liquid state or a more relaxed glassy state<sup>16</sup>. Therefore, the idea of expanded HDA (or eHDA) needs to be re-evaluated.

Furthermore, by quickly recovering HDA through the stability field of ice IX', the formation of LDA (after heating at ambient pressure)

may be the kinetically inhibited result of interrupted crystallization of ice Ih. It may be that if HDA is slowly depressurized, with a substantial pause near 3 kbar, ice IX' may form, followed by ice Ih, thus completing a cycle of stable crystalline phases.

This work experimentally confirms the conceptual framework that indicates that HDA could be a “derailed state along the ice I to ice IV pathway”<sup>24</sup> (here we show that it is the pathway from ice I to ice XV) and confirms the postulation that the formation of HDA is a kinetic event and not a thermodynamic one<sup>5,23,24</sup>. Finally, the interpenetrating and non-interpenetrating nature of the underlying stable crystalline phases of ice may be the principal structural difference between LDA and VHDA. Given that earlier work hinted that the local structure of recovered VHDA and LDA is similar to crystalline forms of ice VI and ice I, respectively (ice VI is the proton-disordered form of ice XV), the full impact of these results can now be appreciated with the demonstration of the formation of the equilibrium crystalline structures under pressure and temperature conditions within the formation zone of HDA. The results imply that a connection between pressure-prepared amorphous ice and deeply supercooled water needs to be re-evaluated. Theoretical studies have also previously questioned the relationship between amorphous ices and liquid water<sup>25–28</sup>. Those studies used molecular dynamics simulations that implied ice-crystallite formation or nucleation, instead of a two-liquid equilibrium, and their results were limited by the timescales of these simulations—a constraint that is essentially removed in our experiment.

### Online content

Any methods, additional references, Nature Research reporting summaries, source data, statements of data availability and associated accession codes are available at <https://doi.org/10.1038/s41586-019-1204-5>.

Received: 26 March 2018; Accepted: 3 April 2019;

Published online 22 May 2019.

- Mishima, O., Calvert, L. D. & Whalley, E. 'Melting ice' I at 77 K and 10 kbar: a new method of making amorphous solids. *Nature* **310**, 393–395 (1984).
- Gallo, P. et al. Water: a tale of two liquids. *Chem. Rev.* **116**, 7463–7500 (2016).
- Tse, J. et al. The mechanisms for pressure-induced amorphization of ice Ih. *Nature* **400**, 647–649 (1999).
- Shephard, J. J. et al. Is high-density amorphous ice simply a “derailed” state along the ice I to ice IV pathway? *J. Phys. Chem. Lett.* **8**, 1645–1650 (2017).
- Strässle, T., Saitta, A. M., Klotz, S. & Braden, M. Phonon dispersion of ice under pressure. *Phys. Rev. Lett.* **93**, 225901 (2004).
- Strässle, T., Klotz, S., Hamel, G., Koza, M. M. & Schober, H. Experimental evidence for a crossover between two distinct mechanisms of amorphization in ice Ih under pressure. *Phys. Rev. Lett.* **99**, 175501 (2007).
- Wang, Y., Zhang, H., Yang, X., Jiang, S. & Goncharov, A. F. Kinetic boundaries and phase transformations of ice I at high pressure. *J. Chem. Phys.* **148**, 044508 (2018).
- Lin, C. L. et al. Kinetically controlled two-step amorphization and amorphous-amorphous transition in ice. *Phys. Rev. Lett.* **119**, 135701 (2017).
- Johari, G. P. Liquid state of low-density pressure-amorphized ice above its  $T_g$ . *J. Phys. Chem. B* **102**, 4711–4714 (1998).
- Seidl, M. et al. Volumetric study consistent with a glass-to-liquid transition in amorphous ices under pressure. *Phys. Rev. B* **83**, 100201 (2011).
- Elsaesser, M. S., Winkel, K., Mayer, E. & Loerting, T. Reversibility and isotope effect of the calorimetric glass → liquid transition of low-density amorphous ice. *Phys. Chem. Chem. Phys.* **12**, 708–712 (2010).
- Giovambattista, N., Angell, C. A., Sciortino, F. & Stanley, H. E. Glass-transition temperature of water: a simulation study. *Phys. Rev. Lett.* **93**, 047801 (2004).
- Lin, C. L., Smith, J. S., Liu, X. Q., Tse, J. S. & Yang, W. G. Venture into water's no man's land: structural transformations of solid H<sub>2</sub>O under rapid compression and decompression. *Phys. Rev. Lett.* **121**, 225703 (2018).
- Finney, J. L. et al. Structure of a new dense amorphous ice. *Phys. Rev. Lett.* **89**, 205503 (2002).
- Tulk, C. A., Hart, R., Klug, D. D., Benmore, C. J. & Neufeind, J. Adding a length scale to the polymorphic ice debate. *Phys. Rev. Lett.* **97**, 115503 (2006).
- Nelmes, R. J. et al. Annealed high-density amorphous ice under pressure. *Nat. Phys.* **2**, 414–418 (2006).
- Kohl, I., Mayer, E. & Hallbrucker, A. Ice XII forms on compression of hexagonal ice at 77 K via high-density amorphous water. *Phys. Chem. Chem. Phys.* **3**, 602–605 (2001).
- Salzmann, C. G., Loerting, T., Kohl, I., Mayer, E. & Hallbrucker, A. Pure ice IV from high-density amorphous ice. *J. Phys. Chem. B* **106**, 5587–5590 (2002).
- Salzmann, C. G., Radaelli, P. G., Hallbrucker, A., Mayer, E. & Finney, J. L. The preparation and structures of hydrogen ordered phases of ice. *Science* **311**, 1758–1761 (2006).

20. Salzmann, C. G. et al. Detailed crystallographic analysis of the ice VI to ice XV hydrogen ordering phase transition. *J. Chem. Phys.* **145**, (2016).
  21. Klotz, S., Hamel, G., Loveday, J. S., Nelmes, R. J. & Guthrie, M. Recrystallisation of HDA ice under pressure by in-situ neutron diffraction to 3.9 GPa. *Z. Kristallogr.* **218**, 117–122 (2003).
  22. Hallbrucker, A., Mayer, E. & Johari, G. P. Glass-transition in pressure-amorphized hexagonal ice: a comparison with amorphous forms made from the vapor and liquid. *J. Phys. Chem.* **93**, 7751–7752 (1989).
  23. Tse, J. S. & Klug, D. D. Pressure amorphized ices – an atomistic perspective. *Phys. Chem. Chem. Phys.* **14**, 8255–8263 (2012).
  24. Tse, J. S. & Klein, M. L. Pressure-induced amorphization of ice I<sub>h</sub>. *J. Chem. Phys.* **92**, 3992–3994 (1990).
  25. Limmer, D. T. & Chandler, D. Theory of amorphous ices. *Proc. Natl Acad. Sci. USA* **111**, 9413–9418 (2014).
  26. Limmer, D. T. & Chandler, D. Comment on “Spontaneous liquid-liquid phase separation of water”. *Phys. Rev. E* **91**, 016301 (2015).
  27. English, N. J. & Tse, J. S. Massively parallel molecular dynamics simulation of formation of ice-crystallite precursors in supercooled water: incipient-nucleation behavior and role of system size. *Phys. Rev. E* **92**, 032132 (2015).
  28. Limmer, D. T. & Chandler, D. Corresponding states for mesostructure and dynamics of super cooled water. *Faraday Discuss.* **167**, 485–498 (2013).
- Acknowledgements** This research used resources at the Spallation Neutron Source, a DOE Office of Science User Facility operated by the Oak Ridge National Laboratory. We thank the Sloan Foundation’s Deep Carbon Observatory for supporting this work.
- Author contributions** C.A.T. conceived and designed the experiment. C.A.T., J.J.M. and A.R.M. conducted the experiment. C.A.T. and D.D.K. analysed the data. C.A.T., D.D.K and C.E.M. wrote the manuscript.
- Competing interests** The authors declare no competing interests.
- Additional information**
- Extended data** is available for this paper at <https://doi.org/10.1038/s41586-019-1204-5>.
- Reprints and permissions information** is available at <http://www.nature.com/reprints>.
- Correspondence and requests for materials** should be addressed to C.A.T.
- Publisher’s note:** Springer Nature remains neutral with regard to jurisdictional claims in published maps and institutional affiliations.
- © This is a U.S. government work and not under copyright protection in the U.S.; foreign copyright protection may apply 2019

## METHODS

The sample-loading techniques that resulted in the formation of the crystalline phases and the amorphous form were identical and proceeded as follows. D<sub>2</sub>O (Sigma Aldrich, 99.99% deuterium) was placed in the lower hemisphere of a single-toroid soft-metal-encapsulated gasket. The gasket was made of a TiZr alloy with a null-scattering composition<sup>29</sup>. The sample and gasket were then placed above boiling liquid nitrogen until the sample froze. The upper portion of the gasket was then placed over the sample. The frozen sample filled the gasket volume completely. In one measurement the gasket contained a small lead pellet to act as a pressure marker. The gasket loaded with ice Ih was then placed between two toroidal cubic boron nitride anvils<sup>30</sup> inside a VX5 Paris–Edinburgh press that was fitted inside a liquid nitrogen cryostat. The anvil's binding rings were modified to include an integrated channel machined into the binding ring to facilitate circulation of liquid nitrogen, thus cooling the sample. A temperature-sensing diode was fixed to the anvil, 3 cm from the sample position. Tests with a second thermocouple embedded in lead and held at the sample position indicated a difference of less than 1 K between the two. A small load was quickly applied after the sample was placed between the anvils to seal the gasket and prevent sample evaporation once the cryostat was evacuated. The Paris–Edinburgh press was placed in the cryostat, which was quickly evacuated, and liquid nitrogen immediately began to flow through the system. The sample was cooled to 100 K over the course of about 30 min.

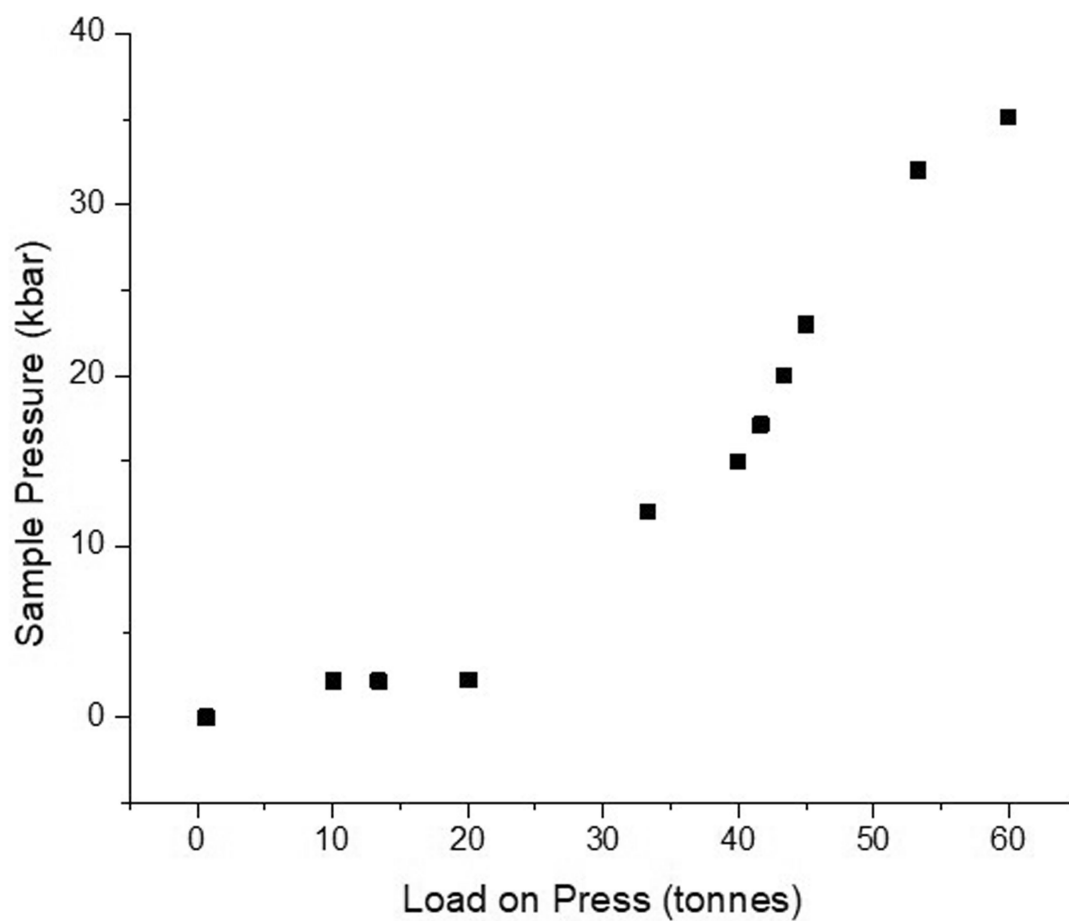
The SNAP instrument at the Spallation Neutron Source at Oak Ridge National Laboratory was configured in low-resolution mode to adequately capture the necessary momentum-transfer range to characterize the HDA form and facilitate the like-for-like comparison with the crystalline phases. Initial data were collected to verify the formation of ice Ih with no phase contamination before any pressure was applied. In the initial experiments a small fraction of the sample was observed to be ice IX, indicating that some pressure had been applied to the sample.

The loading technique was then modified so that no pressure was applied to the sample when sealing the gasket. For each loading, a new D<sub>2</sub>O sample and gasket were used to avoid potential ice IX 'seeds' in the gasket (avoiding any possibility of the ice-memory effect occurring, as has been reported in clathrate hydrate nucleation<sup>31</sup>). Once it was confirmed that ice I was formed with no contaminant phase present, the sample was pressurized in one of two ways. First, the sample pressure was increased to 2 kbar and diffraction data were collected for 1 h. At this point, no ice IX' was found. Then, the pressure was increased to 3 kbar, where we detected the initial formation of ice IX'. Each of these two datasets was measured for 1 h, and the sample pressure was increased into the pressure–temperature field of ice IX over the course of 2 h. This resulted in the formation of the crystalline series reported above. Second, the pressure was increased directly from near-ambient to 15 kbar in just under 30 min. The first dataset was then measured after this direct pressurization into the stability field of ice XV, without first holding the sample pressure in the stability field of ice IX as in the previous experiment. This resulted in the formation of HDA ice.

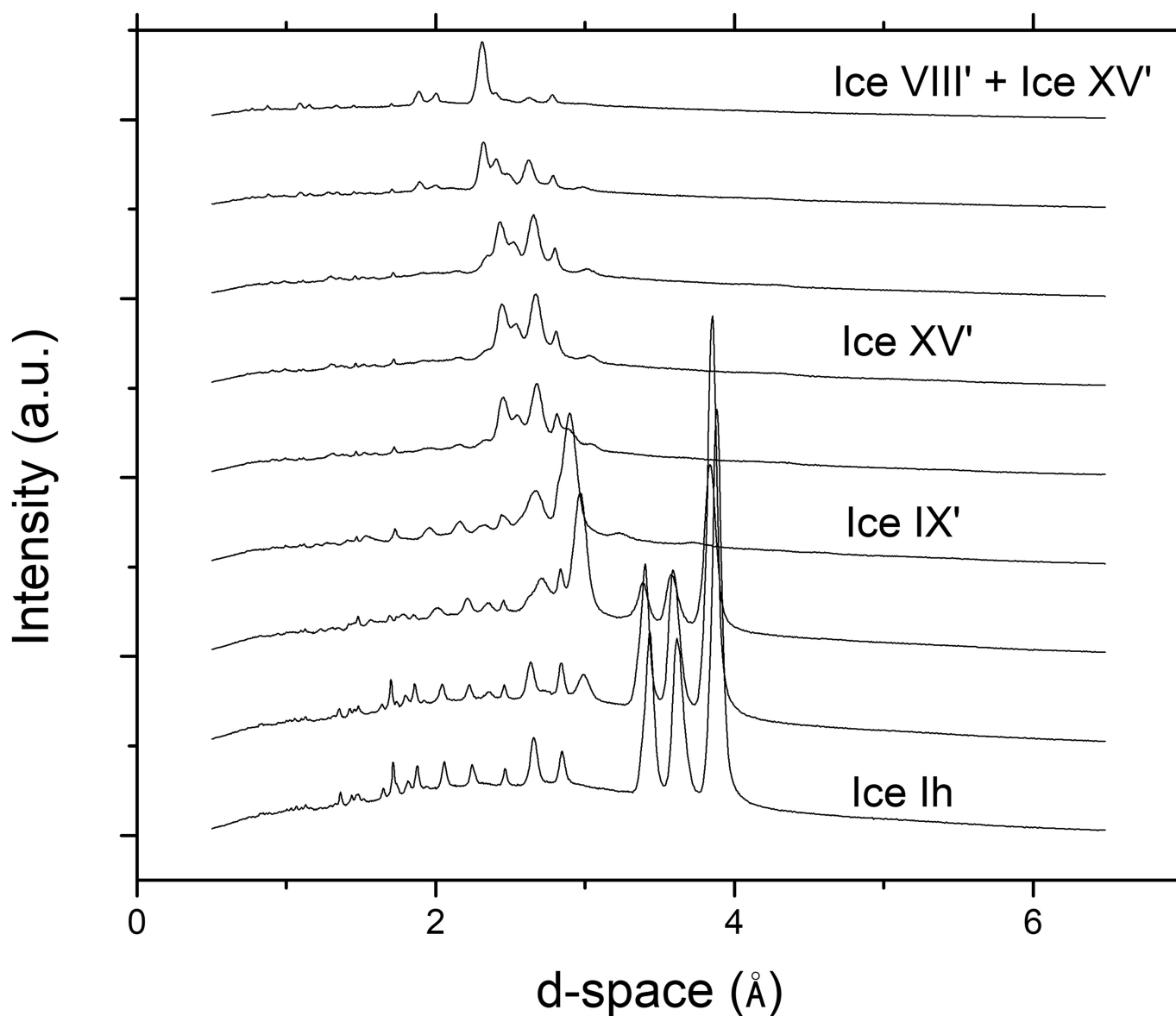
## Data availability

The data that support the findings shown in the figures are available from the corresponding author upon reasonable request.

29. Sidhu, S. S., Heaton, L. R., Zaubers, D. D. & Campos, F. P. Neutron diffraction study of titanium–zirconium system. *J. Appl. Phys.* **27**, 1040–1042 (1956).
30. Khvostantsev, L. G. A verkh–niz (up–down) toroid device for generation of high pressure. *High Temp. High Press.* **16**, 165–169 (1984).
31. Ripmeester, J. A. & Alavi, S. Some current challenges in clathrate hydrate science: nucleation, decomposition and the memory effect. *Curr. Opin. Solid State Mater. Sci.* **20**, 344–351 (2016).

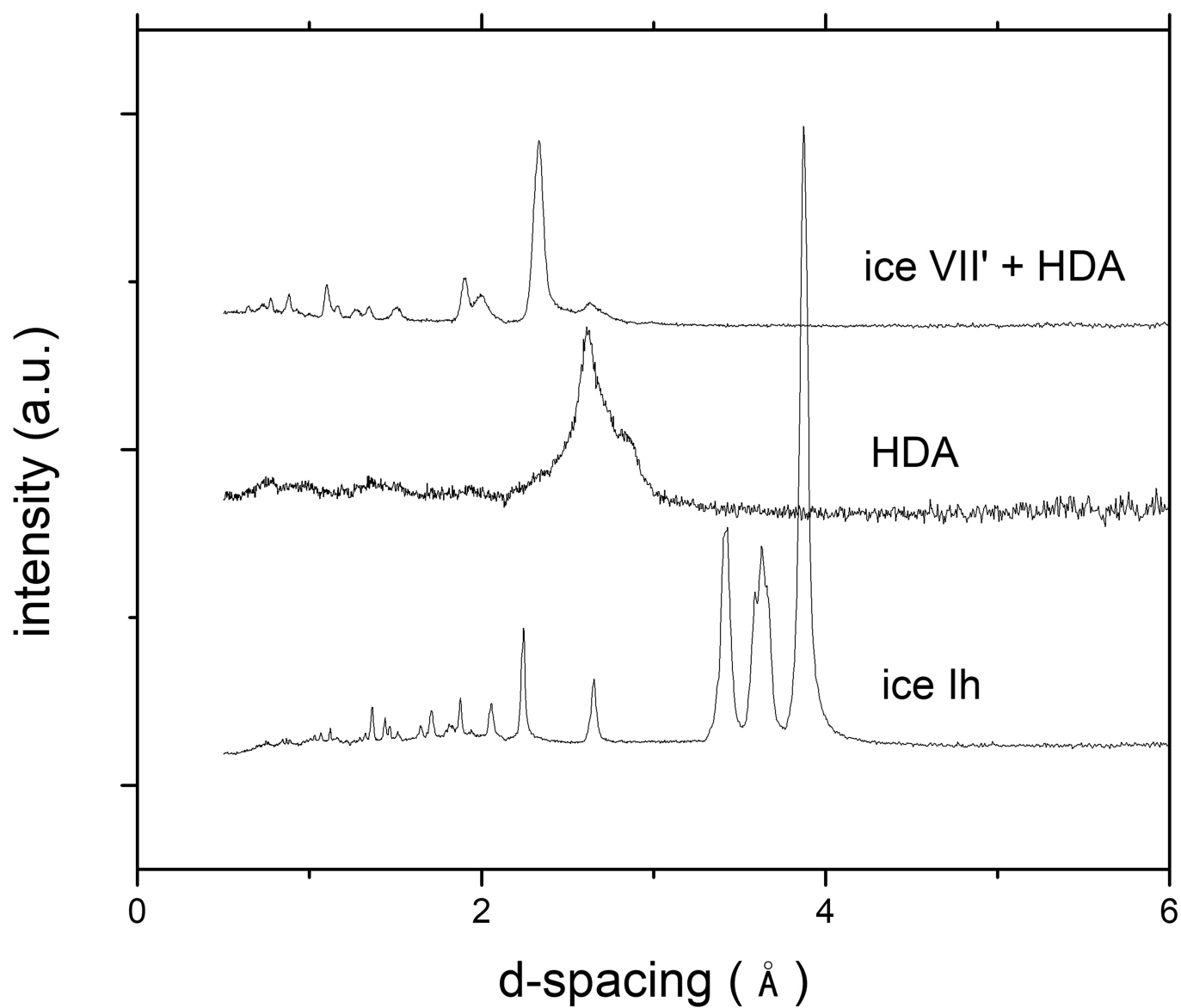


**Extended Data Fig. 1 | Pressure-load curve of a sample mixed with lead.** It should be noted that this curve is not from the dataset presented in Fig. 2, as that sample contained no lead. Thus, no direct one-to-one comparison can be made.



**Extended Data Fig. 2 | Data from separate experimental run, showing the crystallographic transformation sequence.** Initial compression of ice Ih, showing the crystalline sequence of transitions at 100 K. In the initial runs, the cooled sample was predominantly composed of ice Ih with a small amount of ice IX; hence the 'sealing' load that was applied to the gasket was slightly too high, and upon cooling the pressure was such that high-pressure crystalline phases were present. To remove ice IX, the

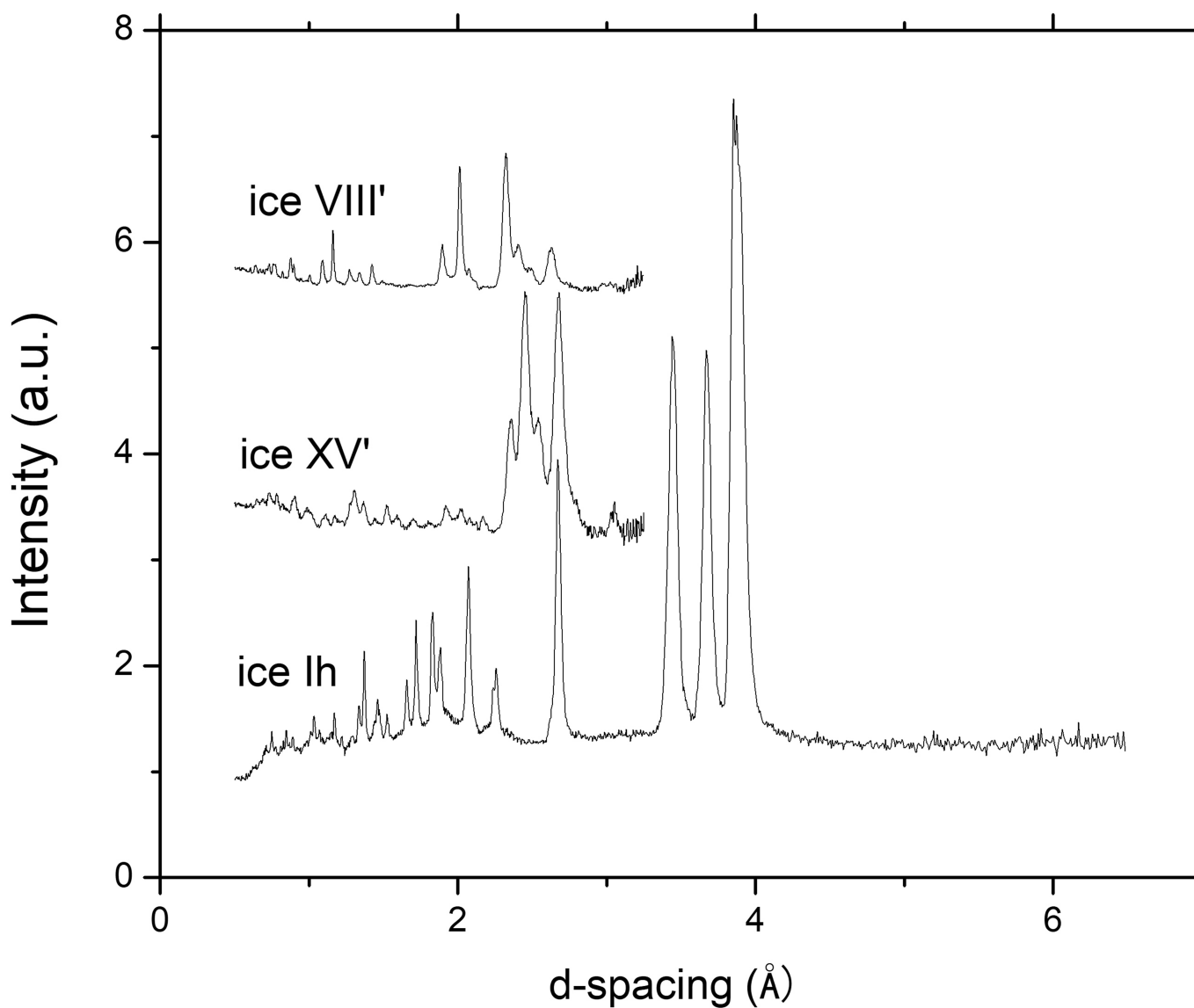
sample was melted at 275 K and the pressure was reduced to atmospheric. Upon re-cooling the sample was determined to be pure ice Ih, as shown in the figure. The data shown in Fig. 2b were obtained from a subsequent loading, with a fresh sample in an unused gasket cooled to 100 K under a small sealing load; no ice IX was found to be present until initial compression at 100 K.



**Extended Data Fig. 3 | *d*-spacing plot of amorphization/recrystallization transformation.** Transformation of pure ice Ih to HDA and recrystallization to ice VII' with some remnant HDA. In this case

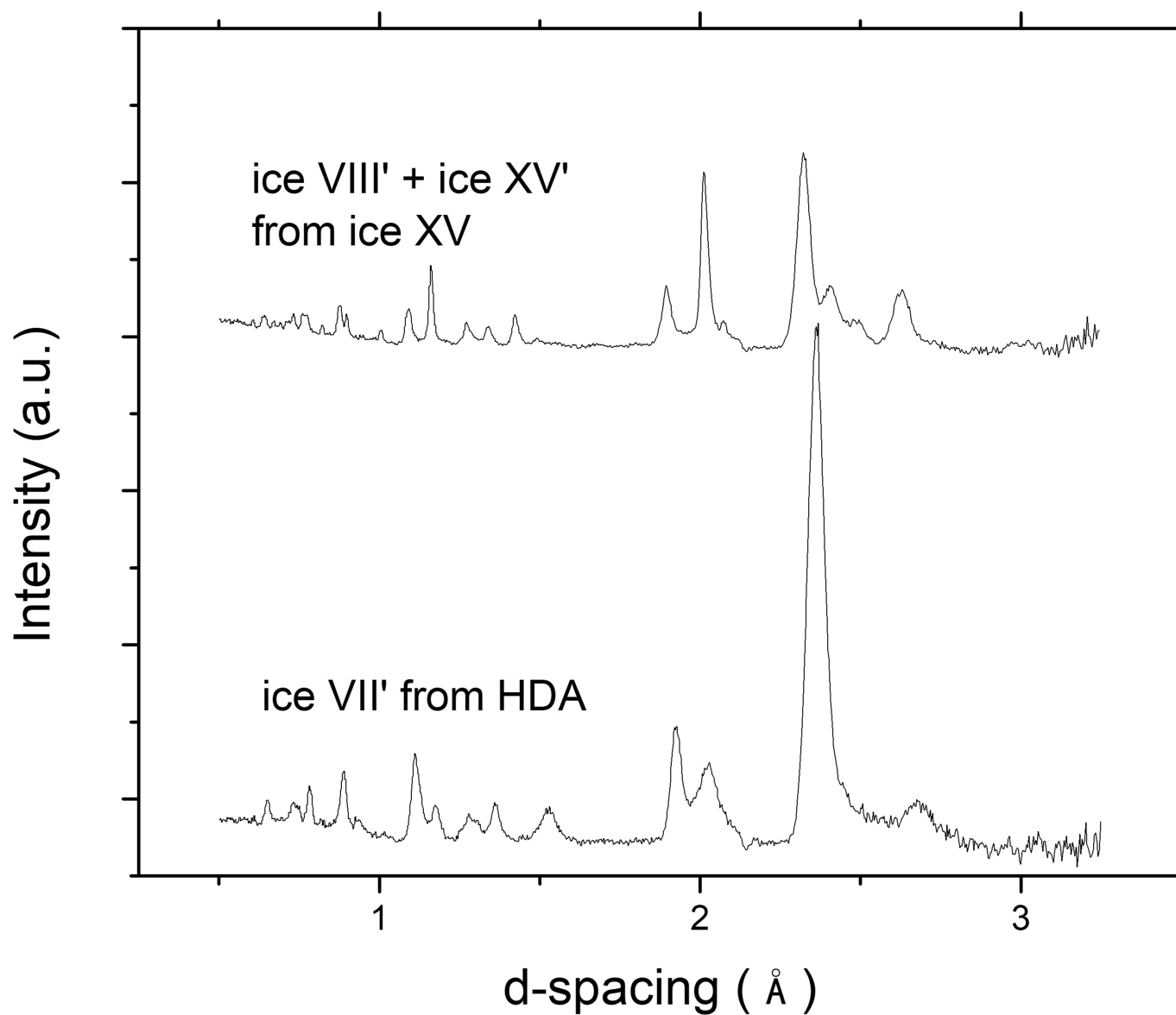
the sample was pressurized directly to 15 kbar in 1,740 s at 100 K. These datasets have been normalized to vanadium.





**Extended Data Fig. 4 | Higher-resolution plot of crystal phases.** Comparison of initial ice Ih with ice XV and ice VIII'. The sample was pressurized slowly with 1-h isobaric breaks to collect diffraction data. The

data were collected using a detector at a greater diffraction angle, thus providing increased resolution at the expense of the momentum-transfer range. These datasets have been normalized to vanadium.



**Extended Data Fig. 5 | Resulting high-pressure crystal phases.** Comparison of the crystal phases resulting from the transformation of ice XV to ice VIII' and from re-crystallization of HDA ice. All datasets were collected at 100 K.